ACS OMEGA

Open Access

http://pubs.acs.org/journal/acsodf

Article

Study on the Photoinduced Isomerization Mechanism of Hydrazone Derivatives Molecular Switch

Xiaojuan Pang,* Kaiyue Zhao, Chenghao Yang, Quanjie Zhong, Ningbo Zhang, and Chenwei Jiang*

Cite This: *ACS Omega* 2025, 10, 17898−17906

Read Online

ACCESS | Metrics & More | Article Recommendations

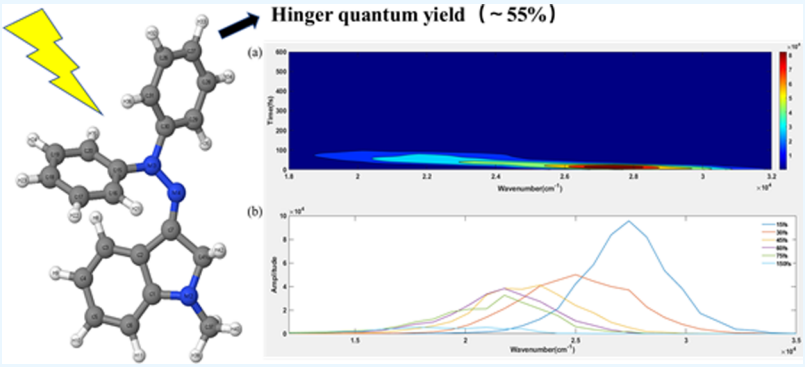

ABSTRACT: Improving quantum yield is an important characteristic for enhancing the operational efficiency of light-driven molecular motors. Building upon Cigan et al.'s pioneering work on CH_3 substitution for H (RSC Adv., 2015, 5, 62449), we have developed a structural modification strategy for hydrazone-based molecular switches through the replacement of a single oxygen atom with two hydrogen atoms, resulting in a remarkable enhancement of the quantum yield. We systematically investigate the photoinduced isomerization mechanism of the hydrazone derivatives molecular switch using the Tully's surface hopping method on the semiempirical OM2/MRCI level. The results show that the calculated quantum yield for the E-to-Z photoisomerization of this molecular rotary motor is approximately (55 ± 3)% (16.01% for original (Pang, X.-J.; Zhao, K.-Y.; He, H.-Y.; Zhang, N.-B.; Jiang, C.-W. Photoinduced isomerization mechanism of isatin N^2-diphenylhydrazones molecular switch. Acta Phys. Sin. 2024, 73 (17).) with an average lifetime of the excited state of 122 fs. Additionally, we calculate the time-dependent fluorescence emission spectra and observe a redshift in wavelength accompanied by fluorescence emission quenching, which shows a blue shift compared to the original isatin N^2-diphenylhydrazone spectrum. Furthermore, we propose that this molecular switch may not have a "dark state".

1. INTRODUCTION

Molecular switches have become a focal point in scientific research due to their ability to respond to external stimuli.[1−4] By means of light irradiation, chemical activation, or electric fields, these switches can achieve precise and reversible transitions between two or more stable states.[1,2,5,6] Molecular switches exhibit significant potential for application, demonstrating a wide range of uses across multiple fields.[6−9] Not only can molecular switches flexibly transition between different states, they can also effectively combine with other functional groups to achieve multifunctional and multiresponsive integration. This combination allows molecular switches to exhibit a more diverse and powerful regulatory capability in complex systems.[6,10] As research advances, molecular switches are expected to give rise to more innovative applications, driving smart molecular technology to new heights. Their broad development prospects and enormous potential inspire great anticipation for their future performance in various cutting-edge scientific fields.[11−15]

The hydrazone-based molecular switch exhibits rapid and precise reversible changes in configuration and conformation in response to chemical activation or photochemical irradiation (light irradiation).[16−19] This rapid response and excellent reversibility make hydrazone-based molecular switches highly promising in various fields.[20−22] Currently, several research groups have published a series of studies on the functional properties of hydrazone-based molecular switches and their derivatives. Cigan et al. reported that the addition of strong anions to benzo hydrazone solutions enhances the deprotonation of the isatin NH group.[23] This results in photoresponsive

Received: January 27, 2025
Revised: March 21, 2025
Accepted: April 15, 2025
Published: April 23, 2025

Scheme 1. (a) Isatin N^2-Diphenylhydrazone Molecular Switch; (b) Modified Hydrazone Derivatives Molecular Switch

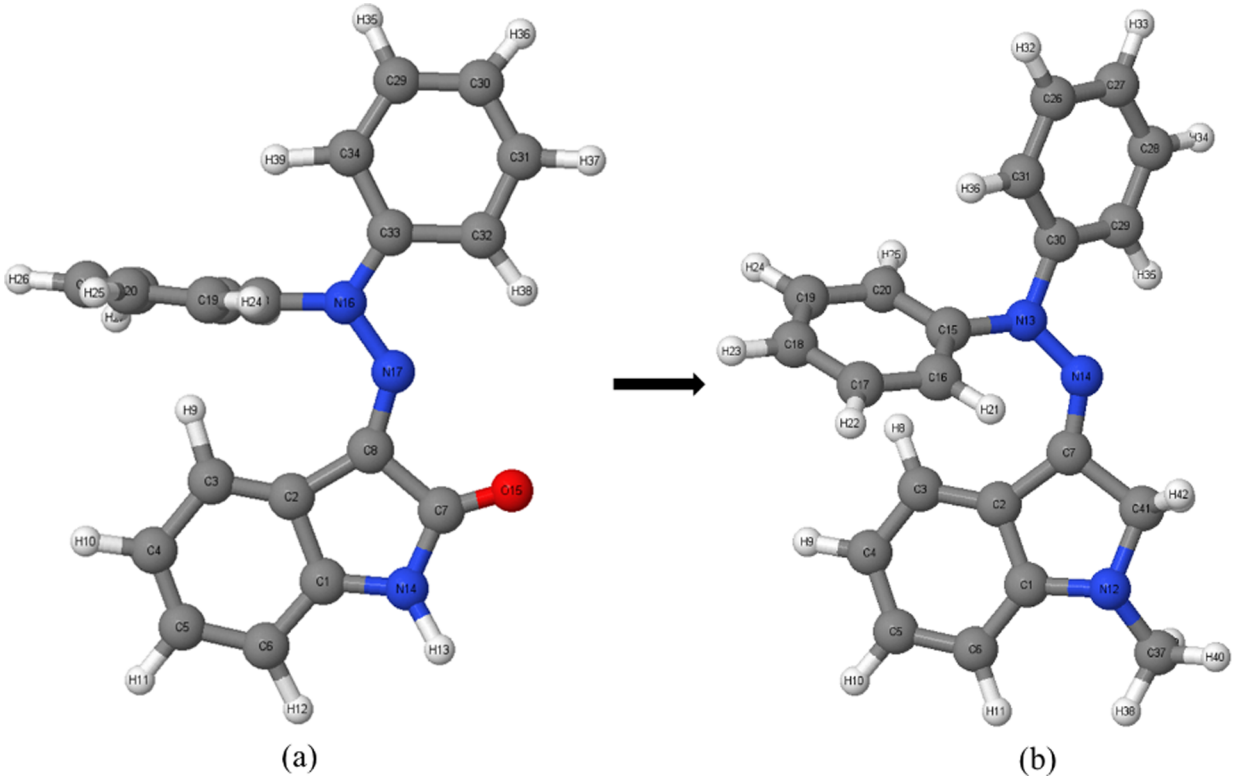

compounds with significant differences in their maximum absorption peaks, demonstrating strong interactions with anions. This characteristic enhances their functionality as molecular switches, enabling them to function as four-state molecular switches within a single molecule.

Tisovský et al. investigated the effects of free metal cations on the photoresponsive switching behavior of diarylhydrazone derivatives of isatin and achieving program-controlled reversible changes.[24] Subsequently, this research group experimentally synthesized a series of photochromic compounds based on indigo and N^2-arylhydrazone derivatives.[19,23] They also studied the synthesis and biological activities of arylhydrazone complexes with various divalent metal cations.[25] In these complex structures, the metal ions prevent the rotation of the ligand around the C═N bond, causing the ligand to lose its on/off functionality. Later, the group reported on the characteristics of isatin bipyridine hydrazone derivatives as molecular switches, as well as the synthesis and Zn-coordination chemistry of their N-anions with bipyridine fragments. They confirmed the optically reversible reaction properties of these molecular switches.[26] The unique properties of hydrazone-based molecular switches hold great promise in various fields, including materials science, optoelectronics, medicine, and chemical sensors. They are expected to play key roles in future technological innovations.[20,27] Through further research and development, hydrazone-based molecular switches hold significant promise for driving technological advancements across various fields. In the future, these molecular switches could provide new pathways for addressing complex scientific problems and enabling efficient applications.

Recently, Cigán et al.[19] designed and synthesized a new isatin N^2-diphenylhydrazone compound. Experiments revealed that this new isatin derivative has different absorption peaks in its E and Z configurations, with their absorption wavelengths in the visible region of the electromagnetic spectrum. Additionally, it was found that rotation around the C═N double bond can occur, enabling photochromic behavior with on/off functionality.[19]

In this study, the basic skeleton of the isatin N^2-diphenylhydrazone compound was modified, design concept as shown in Scheme 1. The motivation for redesigning the molecular geometry stems from the steric and electronic effects of oxygen. We consider the oxygen atom can introduce steric bulk due to their size and the presence of lone pairs. Replacing oxygen with two hydrogens can reduce steric hindrance, allowing for smoother rotational or translational motion within the molecular motor. Oxygen is highly electronegative and can create polar regions within the molecule, potentially leading to unwanted interactions or energy barriers. Replacing oxygen with hydrogen removes these polar effects, which can simplify the energy landscape and facilitate controlled motion.

Research has found that the quantum yield of the modified hydrazone derivative molecular switch here has been significantly improved, increasing from the original unmodified hydrazone derivative molecular 16.01%[28] to (55 ± 3)%. The significant increase in quantum yield for the new molecular switch (with 2 hydrogens replacing 1 oxygen) can be attributed to several factors related to the electronic and structural changes induced by this substitution. Oxygen atoms can cause steric hindrance, which might distort the molecular geometry and lead to less efficient photoisomerization or fluorescence. Hydrogen atoms are smaller and less sterically demanding, allowing the molecule to adopt a more optimal geometry for efficient light emission. The presence of oxygen can complicate the electronic structure of the molecule, leading to a more complex energy landscape with multiple competing excited states. Replacing oxygen with hydrogen simplifies the

https://doi.org/10.1021/acsomega.5c00820
ACS Omega 2025, 10, 17898−17906

electronic structure, potentially leading to a more straightforward and efficient radiative decay process.

To gain deeper insights into the effects of structural modifications, we compared the HOMO (Highest Occupied Molecular Orbital) and LUMO (Lowest Unoccupied Molecular Orbital) electronic orbital diagrams of the unmodified and modified molecular motors. As shown in Scheme 2, replacing

Scheme 2. (a, b) Isatin N^2-Diphenylhydrazone Molecular Switch HOMO and LUMO Electron Orbital Diagrams; (c, d) Modified Isatin N^2-Diphenylhydrazone Molecular Switch HOMO and LUMO Electron Orbital Diagrams

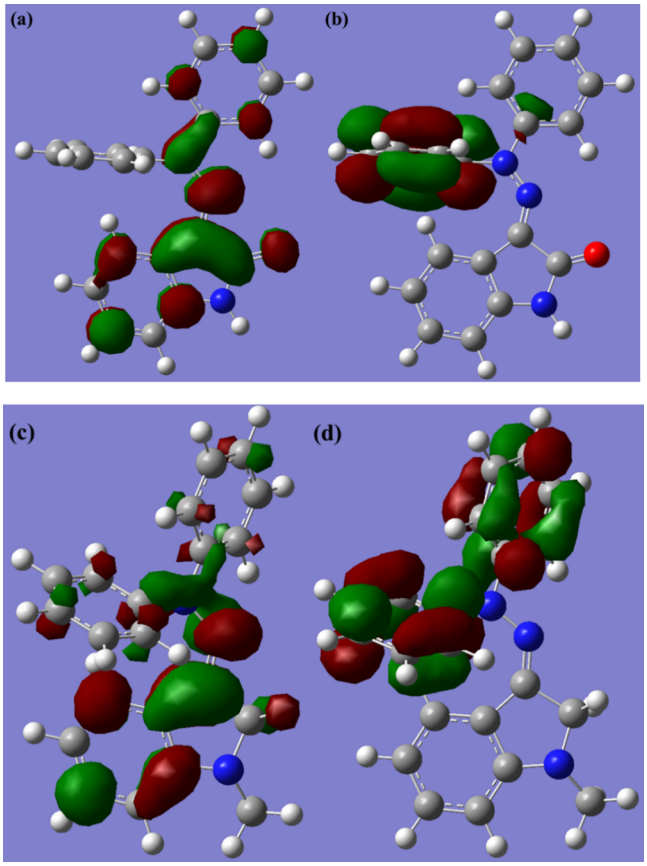

oxygen with hydrogen can enhance the conjugation and delocalization of π-electrons within the molecule. This can lead to a lower energy gap between the ground and excited states, making the radiative transition more favorable and increasing the quantum yield.

Using nonadiabatic orbital-surface hopping molecular dynamics methods at the semiempirical OM2/MRCI level, a detailed mechanism study of this hydrazone derivative as a molecular switch was conducted. The study aimed to reveal the detailed photoisomerization decay mechanism of the molecular motor. Since the molecular system emits photons of specific wavelengths and fluorescence during its de-excitation process, time-resolved fluorescence emission spectra were calculated theoretically to help understand the ultrafast kinetic chemical reaction mechanisms and detect novel reaction phenomena.

2. COMPUTATIONAL DETAILS

The OM2/MRCI method can accurately describe the photo induced process, and the non adiabatic dynamics of OM2/MRCI can provide mechanism explanations that are not obvious in static calculations.[29−34] Therefore, this article investigates the optical driven isomerization of hydrazone derivative molecular motors using the OM2/MRCI method implemented in the MNDO99 program.[35,36] Here, OM2 and MRCI refer to the Orthogonalized Model and Multi-Reference Configuration Interaction, respectively.[33,37]

This paper employs the nonadiabatic dynamics simulation method based on Tully's fewest-switches surface hopping[38] approach to calculate the photochemical isomerization reaction of hydrazone derivative molecular switch.[29,30] The hopping probability is valuated according to the follwing Tully's fewest-swich formula:

$$P_{jk}(t, \mathrm{d}t) \approx \frac{-2\mathrm{d}t}{\rho_{jj}(t)}\mathrm{Re}\left(\rho_{jk}\exp\left[\frac{i}{\hbar}\int_0^t \mathrm{d}t(E_j - E_i)\right]\mathbf{d}_{jk}\cdot\dot{\mathbf{R}}\right)$$

If $P_{ji} < 0$, then the hopping events would not occur.

For $g_{jk}(t, \mathrm{d}t) = \max(P_{jk}(t, \mathrm{d}t),0)$.

In the fewest-switches algorithm, a pseudorandom number ξ uniformly is generated from (0,1), and if it is belonged in the section $\left(\sum_{k=1,k\neq j}^{k-1} g_{jk}, \sum_{k=1,k\neq j}^{k} g_{jk}\right)$, then the hopping events are allowed.

In our calculations, analytic computations of potential energy, energy gradients, and nonadiabatic couplings were performed for both structure optimization and subsequent nonadiabatic dynamics. Additionally, a restricted open-shell Hartree−Fock formalism was applied in the self-consistent field (SCF) treatment. In the MRCI calculations, 14 electrons in 11 orbitals were included in the active space, specifically the seven highest doubly occupied orbitals, the two lowest unoccupied orbitals, and two singly occupied orbitals.[39] Notably, the empirical decoherence correction proposed by Truhlar et al.[40] and Granucci et al.[41] to enhance the fewest switches scheme's internal consistency was not employed in this study.

This study employs the multireference OM2/MRCI method combined with nonadiabatic dynamics simulation techniques to investigate the photochemical isomerization reaction mechanism of hydrazone derivatives molecular switch. Additionally, the quantum yields of photochemical reactions, the state-averaged lifetimes of the molecular switch, the deactivation pathways of the excited state, the fluorescence emission spectra, and red-shifting phenomena were calculated.[29,30,42,43]

Through calculations, we determined that the lowest energies of the E and Z isomers are 3.83 and 4.85 eV, respectively. Given the lower energy of the E isomer, the study here focuses on investigating the isomerization process from E to Z. The nonadiabatic dynamics of the molecule start from the ground state configuration E (as shown in Figure 1) and are performed using Tully's fewest switches surface hopping method. The simulations begin from the S_1state and have a total simulation time of 600 fs. The nuclear evolution time step is set to 0.1 fs, while the electronic evolution time step is set to 0.001 fs. Based on the spectral data in Figure 2, significant differences in the absorption characteristics between the E and Z isomers can be observed. The maximum absorption peaks for the E and Z isomers are 172 nm (7.21 eV) and 202 nm (6.14 eV), respectively, while the minimum absorption peaks for the E and Z isomers are 436 nm (2.84 eV) and 462 nm (2.68 eV), respectively. These differences reflect variations in the electronic structures and molecular orbital distributions of

https://doi.org/10.1021/acsomega.5c00820
ACS Omega 2025, 10, 17898−17906

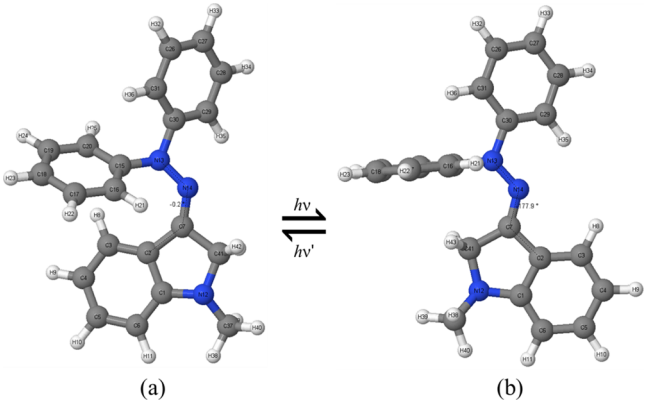

Figure 1. E−Z isomerization mechanism diagram of hydrazone-derivative switch, the optimal configuration diagram of S_0 for the optimal ground state reactant (a) E and product (b) Z, with all relevant atomic numbers marked.

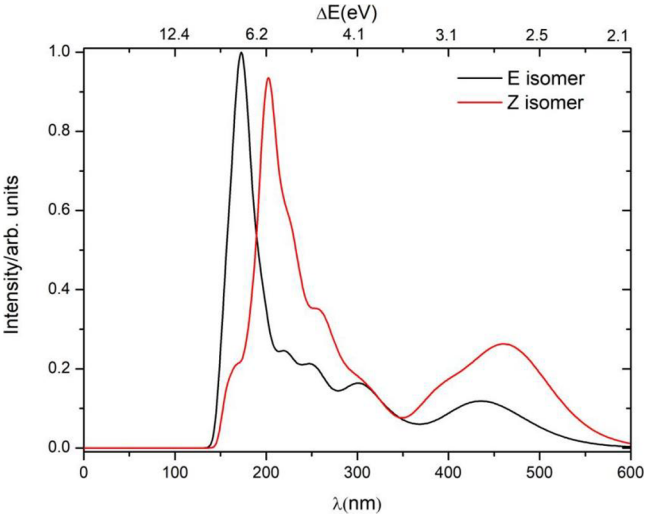

Figure 2. Normalized absorption spectra for the E and Z isomers.

the two isomers, providing important insights into their photophysical.

To gain a deeper understanding of the fluorescence emission spectra, this paper presents time-resolved fluorescence emission spectra during the isomerization process of the molecular switch. In the simulation of the spectra, calculations are based on data sampled from 316 dynamical trajectories. To compute the fluorescence emission intensity at each time point, it is necessary to extract, from 316 initial trajectories obtained via Wigner sampling, information such as the energy, oscillator strength, and current state occupancy at each time step of the nonadiabatic dynamics calculation. According to the spectral calculation theory proposed by Lan et al.,[44,45] the product of the oscillator strength and the number of currently excited states at each time point is cumulatively summed. To ensure both computational speed and accuracy, the simulation summation time step is set to 10 fs. The basic theoretical formulas involved in spectral calculation are presented below.

The scattering cross-section can be represented as

$$\sigma(\omega, t)^{\text{emission}} \propto \omega^2 \int f(\omega, X, t) Q(X, P, t) \mathrm{d}X \mathrm{d}P \tag{1}$$

Among them, X and P represent the atomic coordinates and momenta of the molecule. $Q(X, P, t)$ denotes the phase space distribution function at time t. $f(\omega, X, t)$ represents the oscillator strength of the configuration at time t.

At any given time t, the time-dependent fluorescence emission intensity of hydrazone-derivative switch can be expressed as

$$I(\omega, t)^{\text{emission}} = \omega \cdot \sigma(\omega, t)^{\text{emission}} \tag{2}$$

Substituting eq 1 into eq 2 yields

$$I(\omega, t)^{\text{emission}} \propto \omega^3 \int f(\omega, X, t) Q(X, P, t) \mathrm{d}X \mathrm{d}P \tag{3}$$

In this article, the time-dependent distribution function $Q(X, P, t)$ can be modeled using trajectory propagation evolution. At any time t, the relevant radiation intensity $I(\omega, t)^{\text{emission}}$ can be expressed as

$$I(\omega, t)^{\text{emission}} \propto \omega^3 \sum_{i=1}^{N1} f(\omega_i, t) \delta(\omega - \omega_i) \tag{4}$$

Among them, $f(\omega_i, t)$ is the oscillation intensity of the ith trajectory at time t. It should be noted that the summation here only considers trajectories in the excited state. Because there is no radiation when the molecule is de excited to the ground state. N_1 is the number of configurations in the S_1 excited state. To obtain a smooth spectrum, the function can be broadened using a Gaussian function, where the normalized Gaussian function can be expressed as

$$G(\omega) = G_0 \exp\left[-\frac{(\omega_1 - \omega_i)^2}{2\alpha^2}\right] \tag{5}$$

Among them, set the value of α to 0.05 eV.

The radiation intensity in the time domain and frequency domain can be expressed as

$$I(t)^{\text{emission}} = \int I(\omega, t)^{\text{emission}} \mathrm{d}\omega \tag{6}$$

$$I(\omega)^{\text{emission}} = \int I(\omega, t)^{\text{emission}} \mathrm{d}t \tag{7}$$

3. RESULTS AND DISCUSSION

3.1. Configuration Optimization. To accurately capture the dynamic behavior of the hydrazone derivative molecular switch upon photoexcitation, nonadiabatic dynamics simulations were conducted. Initially, the semiempirical OM2/MRCI method within the MNDO99 software package was employed to optimize the structures of the relevant ground-state molecules. Wigner sampling was used to determine the initial coordinates and velocities of the molecular system for the simulation trajectories.

Next, the molecules were vertically excited to the Franck−Condon (FC) region of the first excited state (S_1), and a 600 fs nonadiabatic dynamics simulation was performed. To further elucidate the molecular configuration changes during the excited state dynamics, the optimized configuration of the molecule in the first excited state (S_1) was analyzed, and its structure is depicted in Figure 3. Meanwhile, to observe the structural changes of the Isatin N^2-diphenylhydrazone molecular switch and the modified hydrazone derivative molecular switch more clearly, we compared the dihedral angle changes of different configurations in the ground state and the excited state, as shown in Table 1. As we can see, the significant dihedral angles of connected central N−N bond

https://doi.org/10.1021/acsomega.5c00820
ACS Omega 2025, 10, 17898−17906

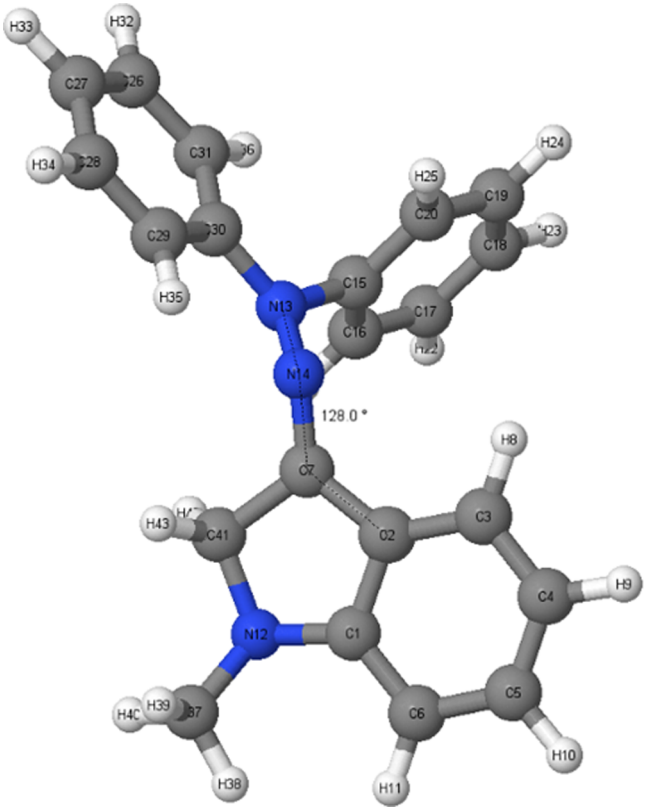

Figure 3. Optimization of the optimal configuration of the first excited state S_1 under the semiempirical OM2/MRCI method of hydrazone-derivative switch.

length and the adjacent dihedral angles for ground S_0 state and S_1 state have noticeable changes, implying a structure changes caused by structural modifications.

The simulation outcomes revealed that the excited-state molecular switch primarily completes the transition back to the ground state through a rotation around the central C═N double bond upon de-excitation. In the specific simulation process, the OM2/MRCI method was combined with Tully's fewest-switches surface-hopping (FSSH) approach. This combination was used to conduct 600 fs molecular dynamics simulations on 316 trajectories initiated from the S_1 FC region."

Among these trajectories, all 316 successfully de-excited back to the ground state within 600 fs, with 173 trajectories undergoing a 360° flip, thus completing the photoisomerization process. This corresponds to a photoisomerization quantum yield of approximately (55 ± 3)% for the hydrazone derivatives molecular switch.

3.2. Nonadiabatic Photoinduced Isomerization Dynamics. In Figure 4a, the black line represents the time-dependent state-averaged occupation number of electrons in the ground state S_0, while the red line shows the same for the first excited state S_1. At 0 fs, electrons are vertically excited to the Franck−Condon region of the first excited state. Consequently, at 0 fs, the state-averaged occupation number in S_1 is 1, and in S_0, it is 0. During the de-excitation process, there is minimal change in the occupation numbers of both states in the first 63 fs. After approximately 326 fs, there are no significant changes in the occupation numbers of the ground and excited states, indicating that all excited-state electrons have returned to the ground state. Notably, between 63 and 326 fs, electrons rapidly de-excite from the first excited state to the ground state. Around 122 fs, there is a crossover where the occupation numbers in the ground and excited states are equal, suggesting an average excited-state lifetime of about 122 fs. As shown in Figure 4b, the single-exponential fitting analysis yielded an average lifetime (τ) of 155 fs, which shows excellent agreement with the theoretically calculated value of 122 fs (Figure 3a).

At the conical intersection point, due to nonradiative transitions, molecules de-excite through two pathways, leading to two different products. One pathway is to the left of the conical intersection gap, where molecules return to their initial ground-state structure upon de-excitation. The other pathway is to the right of the conical intersection gap, where molecules undergo photoisomerization, resulting in the formation of the corresponding isomer.

To better understand the de-excitation process, a statistical plot of the de-excitation times for all 316 trajectories is presented. This plot provides detailed insights into the time scales over which the de-excitation occurs. The de-excitation time is defined as the time it takes for the system to transition from the excited state (S_1) back to the ground state (S_0). In Figure 5, The plot shows the distribution of de-excitation times for 316 trajectories. The *x*-axis represents the de-excitation time (in femtoseconds, fs). The *y*-axis represents the number of trajectories that de-excite within a given time interval. The statistical distribution of these de-excitation times can reveal important information about the dynamics and efficiency of the de-excitation process.

According to Figure 5, a total of 230 trajectories underwent de-excitation between 50 and 150 fs, which aligns with the rapid de-excitation times observed in Figure 4. The statistical plot of de-excitation times for all 316 trajectories provides a comprehensive overview of the de-excitation dynamics in the molecular system. This analysis not only highlights the rapid de-excitation observed in the majority of trajectories but also reveals the existence of slower pathways, contributing to a more complete understanding of the photoisomerization process.

To better illustrate the photoisomerization process, after the nonadiabatic dynamics simulation, the initial and final configurations were extracted from 316 trajectories and analyzed for the dihedral angle $C_2-C_7-N_{14}-N_{13}$. As shown

Table 1. Dihedral Angles of Isatin N^2-Diphenylhydrazone Molecular Switch and Modified Hydrazone Derivatives Molecular Switch Isatin N^2-Diphenylhydrazone Molecular Switch Dihedral Angle

isatin N^2-diphenylhydrazone molecular switch[19]	dihedral angle (S_0)	dihedral angle (S_1)	modified hydrazone derivatives molecular switch	dihedral angle (S_0)	dihedral angle (S_1)
$N_{16}-N_{17}-C_8-C_2$	0°	149.1°	$N_{13}-N_{14}-C_7-C_2$	−0.2°	128.0°
$N_{16}-N_{17}-C_8-C_7$	−180°	−52.4°	$N_{13}-N_{14}-C_7-C_{41}$	13.2°	−74.9°
$C_{18}-N_{16}-N_{17}-C_8$	0°	−74.1°	$C_{15}-N_{13}-N_{14}-C_7$	37.8°	−69.7°
$C_{33}-N_{16}-N_{17}-C_8$	180°	110.1°	$C_{30}-N_{13}-N_{14}-C_7$	−169.4°	138.9°

https://doi.org/10.1021/acsomega.5c00820
ACS Omega 2025, 10, 17898−17906

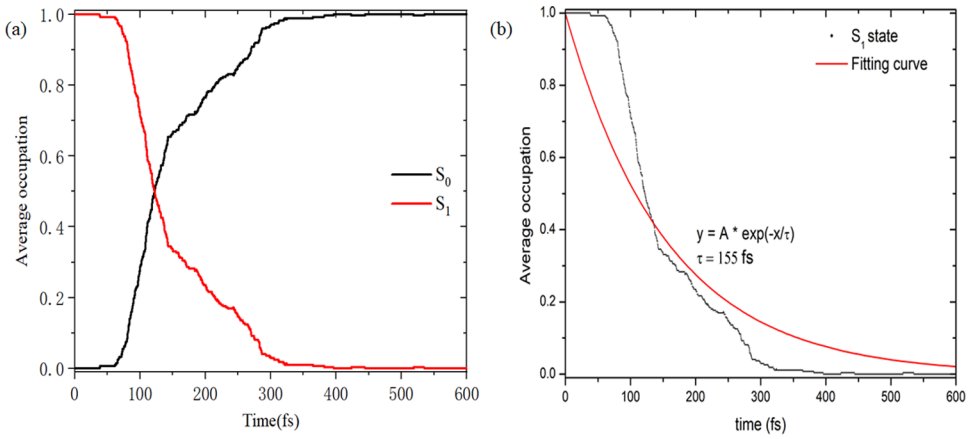

Figure 4. (a) Average occupy of electrons in the S_0 ground state and the first S_1 excited state over time; (b) the fitting curve with a single exponential.

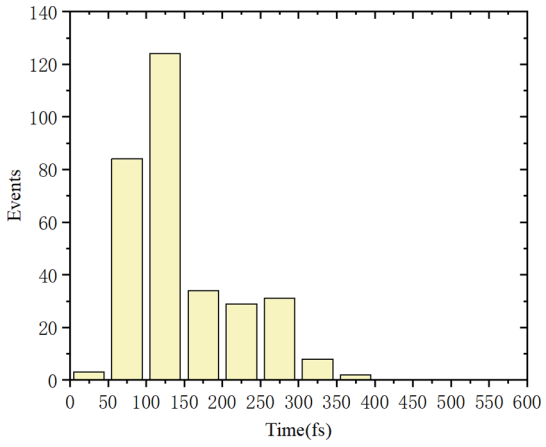

Figure 5. Statistical plot of de-excitation times for all 316 trajectories.

in Figure 6, the dihedral angles of the 316 initial configurations fluctuated around 0°. In the 316 final configurations, 69

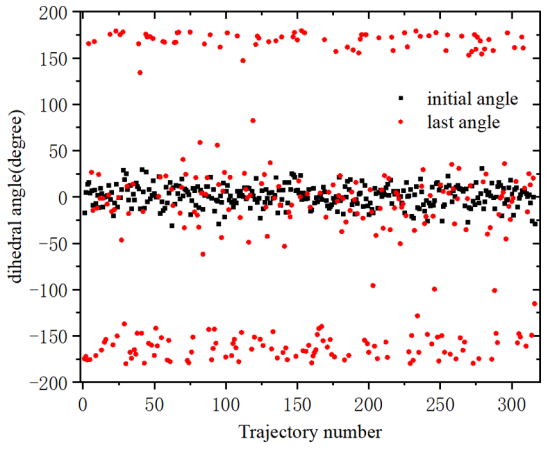

Figure 6. Center dihedral angle $C_2-C_7-N_{14}-N_{13}$ for all initial and final configurations of trajectories.

configurations had dihedral angles around 180°, and 104 configurations had angles around −180°, totaling 173 trajectories that completed isomerization. Meanwhile, 143 final configurations still remained around 0° without significant changes, indicating that these 143 configurations failed to isomerize successfully. These results suggest that the photoisomerization process had a success rate of approximately (55 ± 3)% among the 316 trajectories. Compared to the quantum yield of 16.01% for original isatin N^2-diphenylhydrazone molecular switch,[28] the quantum yield has significantly improved. This analysis not only provides detailed insights into the photoisomerization process but also reveals specific changes in molecular configuration during isomerization.

3.3. Time-Dependent Fluorescence. At 0 fs, the molecular motor absorbs a photon, undergoing a transition from the ground state (S_0) to the first excited state (S_1). Subsequently, it spontaneously relaxes back to the ground state through nonradiative decay. To better understand the fluorescence emission spectrum, the time-resolved fluorescence spectra during the E−Z isomerization process of the molecular switch are shown in Figure 7. In our simulations, calculations were based on a total of 316 trajectories. The two-dimensional contour of fluorescence emission based on oscillator strengths is shown in Figure 7. The *x*-axis and *y*-axis represent wavenumber and time, respectively. As shown in Figure 7a, the values in the blue region of the calculated fluorescence emission spectrum are close to zero. Therefore, the radiation almost disappears after 100 fs. Additionally, the central wavenumber of the deep red, representing the peak intensity of the fluorescence spectrum, is 2.75×10^4 cm^{-1} at 14 fs and approximately 1.37×10^4 cm^{-1} at 97 fs in the fluorescence spectrum, which is much weaker compared to that at 14 fs. Compared to the fluorescence spectrum of the original isatin N^2-diphenylhydrazone molecular switch, this molecular switch exhibits a blue shift in its fluorescence spectrum.

Furthermore, in the time range from 15 to 360 fs, a series of time-evolving emission spectra are fitted to logarithmic normal function lines shown in Figure 7b in different colors. The amplitudes of the fitting lines represent the oscillator strengths at different frequencies. As shown in Figure 7b, the amplitude of the oscillator strength gradually decreases with increasing time, and the wavenumber of each central peak shifts from 9.6 $\times 10^4$ cm^{-1} wavenumbers of 15 fs to smaller 0.5×10^4 cm^{-1} wavenumbers of 150 fs on the left side. Combining the results from Figure 7a, there is more evidence suggesting the presence of wavenumber-resolved redshift in the fluorescence spectra. In summary, wavenumber-resolved redshift and quenching of fluorescence emission occur in the molecular switch system.

https://doi.org/10.1021/acsomega.5c00820
ACS Omega 2025, 10, 17898−17906

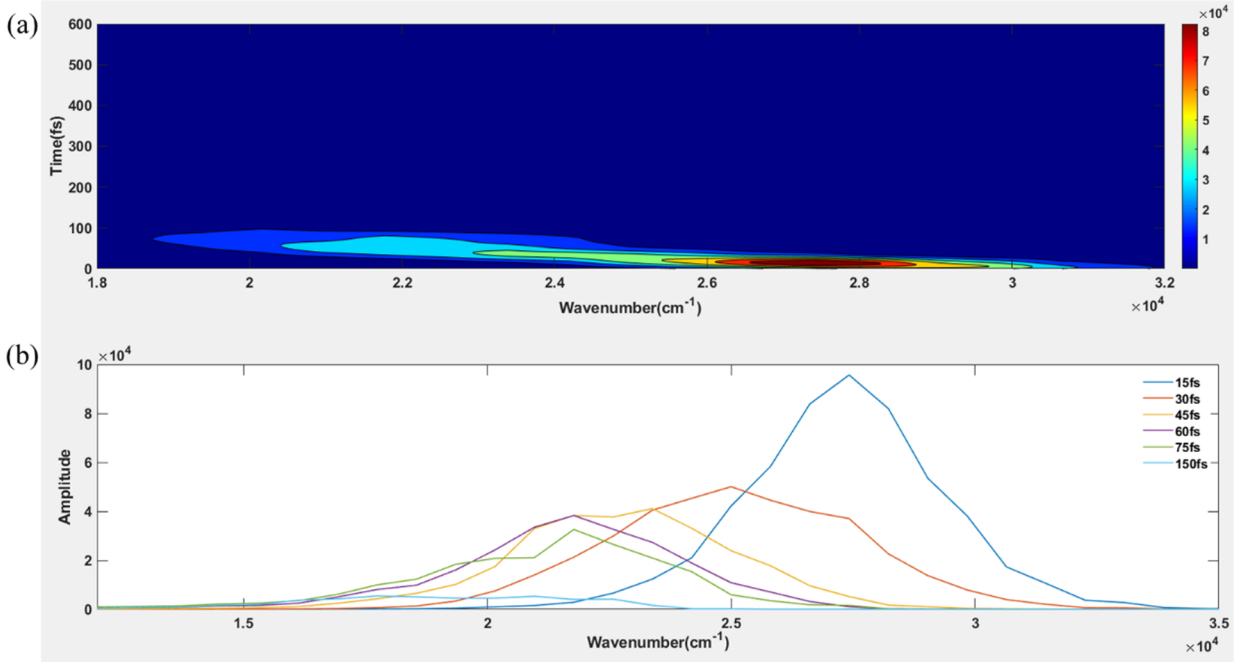

Figure 7. Time-dependent fluorescence emission spectra of excited state dynamics. (a) Time-resolved deconvoluted emission spectrum (b) the wavelength-resolved decay information in different time.

The isatin N^2-diphenylhydrazone molecular switch is predicted to have "dark state" phenomena. However, in the modified molecular motor, fluorescence emission quenching occurs at around 100 fs, which is approximately the time of the average S_1 excited state lifetime of 122 fs. Theoretically, this suggests that there may be no "dark state" phenomena in the photoisomerization process of this molecular motor.

4. CONCLUSIONS

This study employs the trajectory surface hopping dynamics method based on the OM2/MRCI level to investigate the photoinduced isomerization process of hydrazone derivatives molecular switch. Based on nonadiabatic dynamics analysis of 316 trajectories, the research reveals the detailed mechanism of the molecular motor's rotational process. It is found that the quantum yield of E-to-Z photoisomerization is approximately (55 ± 3)%, and the average lifetime of the S_1 excited state is about 122 fs. The computational results indicate that when the molecular motor deactivates from the S_1 state to the S_0 state, it primarily completes the isomerization through a very traditional mechanism. That is, the molecule undergoes a rotational motion with the C═N bond acting as the rotational axis.

Additionally, the average occupation rate over time suggests an average lifetime of about 122 fs. However, the computed time-resolved fluorescence emission spectra show almost no fluorescence emission at 100 fs. It is hypothesized that there may be no "dark state" in the excited state dynamics of the molecular motor during the isomerization process. Furthermore, a red shift in the fluorescence wavelength is observed, which may be indirectly related to the quantum yield of the molecular motor's isomerization. Notably, this molecule exhibits the disappearance of the dark state and a significant increase in quantum yield compared to the original molecular switch. According to the existing results, the disappearance of the dark state may be related to the quantum yield. These findings are of great importance for the future design of more effective molecular switches and motors.

AUTHOR INFORMATION

Corresponding Authors

Xiaojuan Pang − *School of Materials and Physics, China University of Mining & Technology, Xuzhou, Jiangsu 221116, PR China*; Email: xiaojuan.pang@cumt.edu.cn

Chenwei Jiang − *Ministry of Education Key Laboratory for Nonequilibrium Synthesis and Modulation of Condensed Matter, Shaanxi Province Key Laboratory of Quantum Information and Quantum Optoelectronic Devices, School of Physics, Xi'an Jiaotong University, Xi'an, Shaanxi 710049, PR China*; Email: jiangcw@xjtu.edu.cn

Authors

Kaiyue Zhao − *School of Materials and Physics, China University of Mining & Technology, Xuzhou, Jiangsu 221116, PR China*; orcid.org/0009-0005-2158-4265

Chenghao Yang − *School of Materials and Physics, China University of Mining & Technology, Xuzhou, Jiangsu 221116, PR China*

Quanjie Zhong − *School of Materials and Physics, China University of Mining & Technology, Xuzhou, Jiangsu 221116, PR China*; orcid.org/0000-0001-7643-4559

Ningbo Zhang − *School of Mines, China University of Mining & Technology, Xuzhou, Jiangsu 221116, PR China*

Complete contact information is available at: https://pubs.acs.org/10.1021/acsomega.5c00820

Notes

The authors declare no competing financial interest.

ACKNOWLEDGMENTS

This work was supported by the National Natural Science Foundation of China (Grant Nos. 12204532, and 52174137),

https://doi.org/10.1021/acsomega.5c00820
ACS Omega 2025, 10, 17898−17906

the Natural Science Foundation of Jiangsu Province (BK20200648), Key Academic Project of China University of Mining and Technology (Grant No. 2022WLXK16), the Research Start-up Funding of China University of Mining and Technology (Grant No. 102519047), the Graduate innovation project of China University of Mining and Technology (Grant No. 2024WLJCRCZL284). We thank Prof. Zhenggang Lan for providing the programs of MNDO99 and JADE code.

REFERENCES

(1) Shee, S.; Khamaru, K.; Banerji, B. Hydrazone Based pH-Responsive Configurational Molecular Rotary Switches Containing a New Conjugated π-Electronic Framework. *Eur. J. Org. Chem.* **2024**, *27*, No. e202400981.
(2) Leistner, A. L.; Pianowski, Z. L. Smart Photochromic Materials Triggered with Visible Light. *Eur. J. Org. Chem.* **2022**, *2022* (19), No. e202101271.
(3) Janasik, D.; Imielska, P.; Krawczyk, T. Tuning the pH of Activation of Fluorinated Hydrazone-Based Switches—A Pathway to Versatile 19F Magnetic Resonance Imaging Contrast Agents. *ACS Sensors* **2023**, *8* (2), 721−727.
(4) Xu, Y.; Tang, Y.; Li, Q. Visible- and Near-Infrared Light-Driven Molecular Photoswitches for Biological Applications. *Adv. Funct. Mater.* **2024**, No. 2416359.
(5) Pooler, D. R. S.; Lubbe, A. S.; Crespi, S.; Feringa, B. Designing light-driven rotary molecular motors. *CHEM SCI* **2021**, *12* (45), 14964−14986.
(6) Zhang, L.; Wang, H. X.; Li, S.; Liu, M. H. Supramolecular chiroptical switches. *CHEM SOC REV* **2020**, *49* (24), 9095−9120.
(7) Xu, X. N.; Gao, C. Y.; Emusani, R.; Jia, C. C.; Xiang, D. Toward Practical Single-Molecule/Atom Switches. *Adv. Sci.* **2024**, *11* (29), No. 2400877.
(8) Kozlenko, A. S.; Ozhogin, I. V.; Pugachev, A. D.; Lukyanova, M. B.; El-Sewify, I. M.; Lukyanov, B. S. A Modern Look at Spiropyrans: From Single Molecules to Smart Materials. *Top. Curr. Chem.* **2023**, *381* (1), 8.
(9) Fang, L.; Lin, Z.; Zhang, Y.; Ye, B.; Li, J.; Ran, Q.; Wang, X.; Yang, M.; Yuan, Z.; Lin, X.; et al. Robust, Ultrafast and Reversible Photoswitching in Bulk Polymers Enabled by Octupolar Molecule Design. *Angew. Chem., Int. Ed.* **2024**, *63* (16), No. e202402349.
(10) Zhang, B.; Feng, Y. Y.; Feng, W. Azobenzene-Based Solar Thermal Fuels: A Review. *Nano-Micro Lett.* **2022**, *14* (1), 138.
(11) Deng, Y. P.; Long, G. Y.; Zhang, Y.; Zhao, W.; Zhou, G. F.; Feringa, B.; Chen, J. W. Photo-responsive functional materials based on light-driven molecular motors. *Light: Sci. Appl.* **2024**, *13* (1), 63.
(12) Li, Z. Y.; Zeng, X. Y.; Gao, C. M.; Song, J. Z.; He, F.; He, T.; Guo, H.; Yin, J. Photoswitchable diarylethenes: From molecular structures to biological applications. *Coord. Chem. Rev.* **2023**, *497*, No. 215451.
(13) Wang, H.; Bisoyi, H. K.; Zhang, X. F.; Hassan, F.; Li, Q. Visible Light-Driven Molecular Switches and Motors: Recent Developments and Applications. *Chem.—Eur. J.* **2022**, *28* (18), No. e202103906.
(14) Han, Z.; He, M.; Wang, G.; Lehn, J. M.; Li, Q. Visible-Light-Driven Solid-State Fluorescent Photoswitches for High-Level Information Encryption. *Angew. Chem., Int. Ed.* **2024**, *63* (51), No. e202416363.
(15) Wang, H.; Tang, Y.; Krishna Bisoyi, H.; Li, Q. Reversible Handedness Inversion and Circularly Polarized Light Reflection Tuning in Self-Organized Helical Superstructures Using Visible-Light-Driven Macrocyclic Chiral Switches. *Angew. Chem., Int. Ed.* **2023**, *62* (8), No. e202216600.
(16) Ryabchun, A.; Li, Q.; Lancia, F.; Aprahamian, I.; Katsonis, N. Shape-Persistent Actuators from Hydrazone Photoswitches. *J. Am. Chem. Soc.* **2019**, *141* (3), 1196−1200.
(17) Qian, H.; Pramanik, S.; Aprahamian, I. Photochromic Hydrazone Switches with Extremely Long Thermal Half-Lives. *J. Am. Chem. Soc.* **2017**, *139* (27), 9140−9143.
(18) Leigh, D. A.; Marcos, V.; Nalbantoglu, T.; Vitorica-Yrezabal, I. J.; Yasar, F. T.; Zhu, X. Pyridyl-Acyl Hydrazone Rotaxanes and Molecular Shuttles. *J. Am. Chem. Soc.* **2017**, *139* (20), 7104−7109.
(19) Cigán, M.; Gáplovsky, M.; Jakusová, K.; Donovalová, J.; Horváth, M.; Filo, J.; Gáplovsky, A. Isatin N2-diphenylhydrazones: new easily synthesized Vis-Vis molecular photoswitches†. *RSC Adv.* **2015**, *5* (77), 62449−62459.
(20) Murugappan, S.; Dastari, S.; Jungare, K.; Barve, N. M.; Shankaraiah, N. Hydrazide-hydrazone/hydrazone as enabling linkers in anti-cancer drug discovery: A comprehensive review. *J. Mol. Struct.* **2024**, *1307*, No. 138012.
(21) Schnetz, M.; Meier, J. K.; Rehwald, C.; Mertens, C.; Urbschat, A.; Tomat, E.; Akam, E. A.; Baer, P.; Roos, F. C.; Brüne, B. The Disturbed Iron Phenotype of Tumor Cells and Macrophages in Renal Cell Carcinoma Influences Tumor Growth. *Cancers* **2020**, *12* (3), 530.
(22) Shao, B. H.; Aprahamian, I. Hydrazones as New Molecular Tools. *Chem.* **2020**, *6* (9), 2162−2173.
(23) Cigán, M.; Jakusová, K.; Gáplovsky, M.; Filo, J.; Donovalová, J.; Gáplovsky, A. Isatin phenylhydrazones: anion enhanced photochromic behaviour†. *Photochem. Photobiol. Sci.* **2015**, *14* (11), 2064−2073.
(24) Tisovsky, P.; Donovalova, J.; Kozisek, J.; Horvath, M.; Gaplovsky, A. Reversible ON/OFF and OFF/ON, light-stimulated binding, or release processes of metal cations from isatin diarylhydrazone complexes in solution. *J. Photochem. Photobiol., A* **2022**, *427*, No. 113827.
(25) Seleem, H. S. Transition metal complexes of an isatinic quinolyl hydrazone. *Chem. Cent. J.* **2011**, *5*, 35.
(26) Sandrik, R.; Tisovsky, P.; Csicsai, K.; Donovalová, J.; Gáplovsky, M.; Sokolík, R.; Filo, J.; Gáplovsky, A. ON/OFF Photostimulation of Isatin Bipyridyl Hydrazones: Photochemical and Spectral Study. *Molecules* **2019**, *24* (14), 2668.
(27) Su, X.; Aprahamian, I. Hydrazone-based switches, metallo-assemblies and sensors. *CHEM SOC REV* **2014**, *43* (6), 1963−1981.
(28) Pang, X.-J.; Zhao, K.-Y.; He, H.-Y.; Zhang, N.-B.; Jiang, C.-W. Photoinduced isomerization mechanism of isatin N < sup > 2</sup>-diphenylhydrazones molecular switch. *Acta Phys. Sin.* **2024**, *73* (17), 173101.
(29) Pang, X. J.; Zhao, K. Y.; Hu, D. P.; Zhong, Q. J.; Zhang, N. B.; Jiang, C. W. Effect of load-resisting force on photoisomerization mechanism of a single second generation light-driven molecular rotary motor. *J. Chem. Phys.* **2024**, *161* (16), 164302.
(30) Pang, X. J.; He, H. Y.; Zhao, K. Y.; Zhang, N. B.; Zhong, Q. J. Ultrafast nonadiabatic photoisomerization dynamics study of molecular motor based on the synthetic indanylidene-ppyrrolinium frameworks. *Chem. Phys. Lett.* **2023**, *819*, No. 140439.
(31) Pang, X. J.; Cui, X. Y.; Hu, D. P.; Jiang, C. W.; Zhao, D.; Lan, Z. G.; Li, F. L. "Watching" the Dark State in Ultrafast Nonadiabatic Photoisomerization Process of a Light-Driven Molecular Rotary Motor. *Journalof Physical Chemistry. A* **2017**, *121* (6), 1240−1249.
(32) Zhuang, X. H.; Wang, J.; Lan, Z. G. Photoinduced Nonadiabatic Decay and Dissociation Dynamics of Dimethylnitramine. *Journalof Physical Chemistry. A* **2013**, *117* (23), 4785−4793.
(33) Weber, W.; Thiel, W. Orthogonalization corrections for semiempirical methods. *Theor. Chem. Acc.* **2000**, *103* (6), 495−506.
(34) Otte, N.; Scholten, M.; Thiel, W. Looking at Self-Consistent-Charge Density Functional Tight Binding from a Semiempirical Perspective. *Journalof Physical Chemistry. A* **2007**, *111* (26), 5751−5755.
(35) Thiel, W. The MNDOC Method, a Correlated Version of the MNDO Model. *J. Am. Chem. Soc.* **1981**, *103* (6), 1413−1420.
(36) Wang, J.; Durbeej, B. Toward Fast and Efficient Visible-Light-Driven Molecular Motors:A Minimal Design. *ChemistryOpen* **2018**, *7* (8), 583−589.
(37) Koslowski, A.; Beck, M. E.; Thiel, W. Implementation of a general multireference configuration interaction procedure with analytic gradients in a semiempirical context using the graphical

https://doi.org/10.1021/acsomega.5c00820
ACS Omega 2025, 10, 17898−17906

unitary group approach. *Journal Of Computational Chemistry* **2003**, *24* (6), 714−726.
(38) Tully, J. C. Molecular dynamics with electronic transitions. *J. Chem. Phys.* **1990**, *93* (2), 1061−1071.
(39) Ma, J. Z.; Yang, S. J.; Zhao, D.; Jiang, C. W.; Lan, Z. G.; Li, F. L. Orthogonalization corrections for semiempirical methods. *Theor. Chem. Acc.* **2022**, *103* (7), 495−506.
(40) Zhu, C. Y.; Jasper, A. W.; Truhlar, D. G. Non-Born-Oppenheimer Liouville-von Neumann dynamics. Evolution of a subsystem controlled by linear and population-driven decay of mixing with decoherent and coherent switching. *J. Chem. Theory Comput.* **2005**, *1* (4), 527−540.
(41) Granucci, G.; Persico, M.; Zoccante, A. Including quantum decoherence in surface hopping. *J. Chem. Phys.* **2010**, *133* (13), 134111.
(42) Pios, S. V.; Gelin, M. F.; Ullah, A.; Dral, P. O.; Chen, L. Artificial-Intelligence-Enhanced On-the-Fly Simulation of Nonlinear Time-Resolved Spectra. *Journal Of Physical Chemistry Letters* **2024**, *15*, 2325−2331.
(43) Conti, I.; Cerullo, G.; Nenov, A.; Garavelli, M. Ultrafast Spectroscopy of Photoactive Molecular Systems from First Principles: Where We Stand Today and Where We Are Going. *J. Am. Chem. Soc.* **2020**, *142* (38), 16117−16139.
(44) Lan, Z. G.; Lu, Y.; Weingart, O.; Thiel, W. Nonadiabatic Decay Dynamics of a Benzylidene Malononitrile. *Journalof Physical Chemistry. A* **2012**, *116* (6), 1510−1518.
(45) Jin, H.; Liang, M.; Arzhantsev, S.; Li, X.; Maroncelli, M. Photophysical Characterization of Benzylidene Malononitriles as Probes of Solvent Friction. *Journalof Physical Chemistry. B* **2010**, *114* (22), 7565−7578.

https://doi.org/10.1021/acsomega.5c00820
ACS Omega 2025, 10, 17898−17906